Structure of CD84 provides insight into SLAM family function

Qingrong Yan[†], Vladimir N. Malashkevich[‡], Alexander Fedorov[‡], Elena Fedorov[‡], Erhu Cao[†], Jeffrey W. Lary[§], James L. Cole[§], Stanley G. Nathenson[†¶‖], and Steven C. Almo[‡‖††]

Departments of [†]Cell Biology, [¶]Microbiology and Immunology, [‡]Biochemistry, and [††]Physiology and Biophysics, Albert Einstein College of Medicine, Bronx, NY 10461; and [§]National Analytical Ultracentrifugation Facility, University of Connecticut, Biotechnology/Bioservices Center Unit 3149, Storrs, CT 06269

Contributed by Stanley G. Nathenson, April 30, 2007 (sent for review April 10, 2007)

The signaling lymphocyte activation molecule (SLAM) family includes homophilic and heterophilic receptors that modulate both adaptive and innate immune responses. These receptors share a common ectodomain organization: a membrane-proximal immunoglobulin constant domain and a membrane-distal immunoglobulin variable domain that is responsible for ligand recognition. CD84 is a homophilic family member that enhances IFN-γ secretion in activated T cells. Our solution studies revealed that CD84 strongly self-associates with a K_d in the submicromolar range. These data, in combination with previous reports, demonstrate that the SLAM family homophilic affinities span at least three orders of magnitude and suggest that differences in the affinities may contribute to the distinct signaling behavior exhibited by the individual family members. The 2.0 Å crystal structure of the human CD84 immunoglobulin variable domain revealed an orthogonal homophilic dimer with high similarity to the recently reported homophilic dimer of the SLAM family member NTB-A. Structural and chemical differences in the homophilic interfaces provide a mechanism to prevent the formation of undesired heterodimers among the SLAM family homophilic receptors. These structural data also suggest that, like NTB-A, all SLAM family homophilic dimers adopt a highly kinked organization spanning an end-to-end distance of ≈140 Å. This common molecular dimension provides an opportunity for all two-domain SLAM family receptors to colocalize within the immunological synapse and bridge the T cell and antigen-presenting cell.

homophilic | dimer | affinity

Members of the signaling lymphocyte activation molecule (SLAM) family modulate a wide range of immune responses, including T cell activation, memory B cell generation, antibody production, and natural killer cell activation (1). The genes encoding SLAM family members, including SLAM (CD150), NTB-A (SLAM6), CD84, 19A (CRACC), Ly-9 (CD229), 2B4 (CD244), CD48, SLAMF8, and SLAMF9 (2, 3), are tightly clustered on human chromosome 1 at 1q23 and mouse chromosome 1 at 1H2 (4). The SLAM family is a subset of the CD2 family, which also includes CD2 and CD58 located on chromosome 1 at 1p13 in humans. In mice, CD2 is located on chromosome 3 (5), and there is no CD58 homologue. The SLAM/CD2 family members share a similar ectodomain organization, with a membrane-distal immunoglobulin variable (IgV) domain that is responsible for ligand recognition and a membrane-proximal truncated immunoglobulin constant-2 (IgC2) domain. The sole exception is the Ly-9, which contains a tandem repeat of the IgV-IgC2 motif. It is notable that the binding partners of all characterized SLAM/CD2 family members are from the same family, and there exist both homophilic (e.g., CD150, CD84, Ly9, and NTB-A bind with themselves) and heterophilic interactions (e.g., 2B4 binds with CD48, and CD2 binds with CD58) (4).

Elements of the signaling pathways initiated by engagement of the SLAM family receptors operate through the SLAM-associated protein (SAP) and the related EWS-activated transcript 2 (EAT-2). Missense mutations in SAP that impair interactions with SLAM family receptors affect processes involving $CD4^+$ and $CD8^+$ T cells, natural killer cells, natural killer T cells, B cells, and platelets. In particular, defects in SAP are associated with inherited X-linked lymphoproliferative syndrome, which is characterized by a dysregulated immune response to infection by Epstein–Barr virus, B cell lymphomas, and dysgammaglobulinemia (4). Notably, blockade of 2B4 in wild-type cytotoxic T lymphocytes results in defects analogous to those observed in SAP-deficient cytotoxic T lymphocytes (6). Furthermore, CD150-, NTB-A-, and Ly-9-deficient mice also show similar T cell defects (7–9).

Of particular note is CD84, a homophilic receptor expressed on T cells, B cells, dendritic cells, monocytes, macrophages, eosinophils, mast cells, granulocytes, and platelets. CD84 expression increases the following activation of T cells, B cells, and dendritic cells (1). Treatment of human T cells with CD84-Ig enhances TCR-induced IFN-γ secretion presumably through homophilic engagement of cell surface CD84 (10). It has also been demonstrated that CD84 homophilic engagement induces platelet stimulation (11).

Our analytical ultracentrifugation (AUC) analyses of CD84 revealed a strong self-association with a K_d in the submicromolar range. In combination with previously published work (12, 13), the current study demonstrated that the homophilic affinities span at least three orders of magnitude. This finding suggested that differences in affinities might be a contributor to the different signaling behavior exhibited by the individual family members. The 2.0-Å crystal structure of the human CD84 IgV domain revealed a twofold symmetric homophilic dimer formed by the orthogonal association of front β-sheets from the interacting IgV domains. The CD84 homophilic interaction exhibited significant overall similarity with the recently published NTB-A homophilic dimer. Notably, the physical and chemical properties of the surfaces contributing to the dimer interfaces provide a potential mechanism to prevent unwanted heterodimerization (12). The NTB-A and CD84 crystal structures provide models for other homophilic interactions in the SLAM family.

Results

CD84 Is Dimeric in Solution. Refolded CD84 ectodomain (22,385 Da) and IgV domain (12,646 Da) both eluted as symmetric

Author contributions: Q.Y., E.C., S.G.N., and S.C.A. designed research; Q.Y., V.N.M., A.F., E.F., J.W.L., and J.L.C. performed research; Q.Y. contributed new reagents/analytic tools; Q.Y., V.N.M., J.W.L., and J.L.C. analyzed data; and Q.Y. wrote the paper.

The authors declare no conflict of interest.

Abbreviations: AUC, analytical ultracentrifugation; SLAM, signaling lymphocyte activation molecule; IgV, immunoglobulin variable; IgC, immunoglobulin constant; APC, antigen-presenting cell; Sc, shape complementarity.

Data deposition: The structure factors and coordinates reported in this paper have been deposited in the Protein Data Bank, www.pdb.org (PDB ID code 2PKD).

‖To whom correspondence may be addressed. E-mail: nathenso@aecom.yu.edu or almo@aecom.yu.edu.

This article contains supporting information online at www.pnas.org/cgi/content/full/0703893104/DC1.

© 2007 by The National Academy of Sciences of the USA

monodisperse peaks on calibrated gel-filtration columns, with apparent molecular masses of 60 kDa and 32 kDa, respectively [supporting information (SI) Fig. 5]. These data suggested that CD84 is not monomeric in solution. A more quantitative assessment of the oligomeric state was provided by sedimentation velocity analysis. The observation that the normalized sedimentation factor g(s*) plots superimpose is strong evidence that, over the concentration range examined, reversible dissociation is not occurring (14, 15) (Fig. 1). Analysis of the complete data sets with Sedphat version 4.04 (16), using the model of a single ideal species, yielded molecular masses of 23.9 kDa and 44.1 kDa for the CD84 IgV domain and full-length ectodomain, respectively. These results indicated that over the concentration ranges studied both the IgV and the complete CD84 ectodomain exist as dimers (expected dimer molecular masses of 25.3 and 44.8 kDa, respectively), with no indication of dissociation to monomers or further aggregation beyond the dimers. The lack of detectable dissociation, over the concentration range examined, sets the upper limit for the K_d at several hundred nanomolars.

SLAM Family Members Possess a Noncanonical IgV Domain. The asymmetric unit in the CD84 crystals contains six independent copies of the CD84 IgV domain (Fig. 2*A*), which exhibits the classic two-layer β-sandwich topology present in other IgV structures. The front and back sheets of the domain are composed of the A′GFCC′C″ and BED strands, respectively (Fig. 2*B*). The six independent molecules are substantially similar with each other: Pairwise comparisons resulted in rms deviations ranging from 0.44 Å to 0.79 Å (based on 103 C_α atoms), with the BC, C′C″, and FG loops exhibiting the greatest variability (Fig. 2*B*). Two notable features are present in the CD84 IgV domain. Canonical IgV domains start with the A strand, followed by the A′ strand, which form hydrogen bonds with the B and G strands, respectively; however, the N terminus of the CD84 IgV domain lacks the equivalent of the A strand and begins with the A′ strand. Furthermore, the hallmark disulfide bond that links the B and F strands in canonical IgV domains is absent in CD84. Based on sequence analysis, both of these unique features are predicted to be present in all SLAM/CD2 family members and, in fact, have been directly observed in CD2, CD58 (17), 2B4 (18), and NTB-A (12).

CD84 Forms Two Types of Dimers in the Crystalline State. The six molecules in the asymmetric unit form two distinct interfaces. Head-to-tail dimers, involving the approximately orthogonal association of front-sheet strands (GFCC′C″), are formed by the interaction of molecules A with B, molecules C with E, and molecules D with F (Fig. 2*A*). These three independent dimers are very similar with rms deviations that range from 0.6 to 0.8 Å. Parallel, side-to-side dimers, formed by the association of molecules A with C, molecules B with D, and molecules F with the symmetry mate E′, are stabilized by interfaces formed by strands on the back sheet (A′B) (SI Fig. 6). The rms deviations among the side-to-side dimers range from 0.82 to 1.14 Å. Given the similarities, only the AB head-to-tail dimer and the AC side-to-side dimer are discussed unless noted.

The head-to-tail dimers are roughly twofold symmetric, with the interacting sheets crossing at a nearly orthogonal angle and burying ≈1,460 to 1,480 Å^2 of solvent-accessible surface area. This interface is composed predominantly of neutral polar residues, which participate in 14 hydrogen bonds and a number of van der Waals contacts (Fig. 2*C* and SI Table 1). No salt bridges contribute to this interface. Two predominant types of interactions, loop-to-strand and strand-to-strand, can be defined across this dimer interface. The strand-to-loop class includes side-chain-to-side-chain contacts formed by T38 and S39 on the CC′ loop from molecule A with A33 on the C strand and D90 on the F strand from molecule B; and T57, H58, R59, and Y62

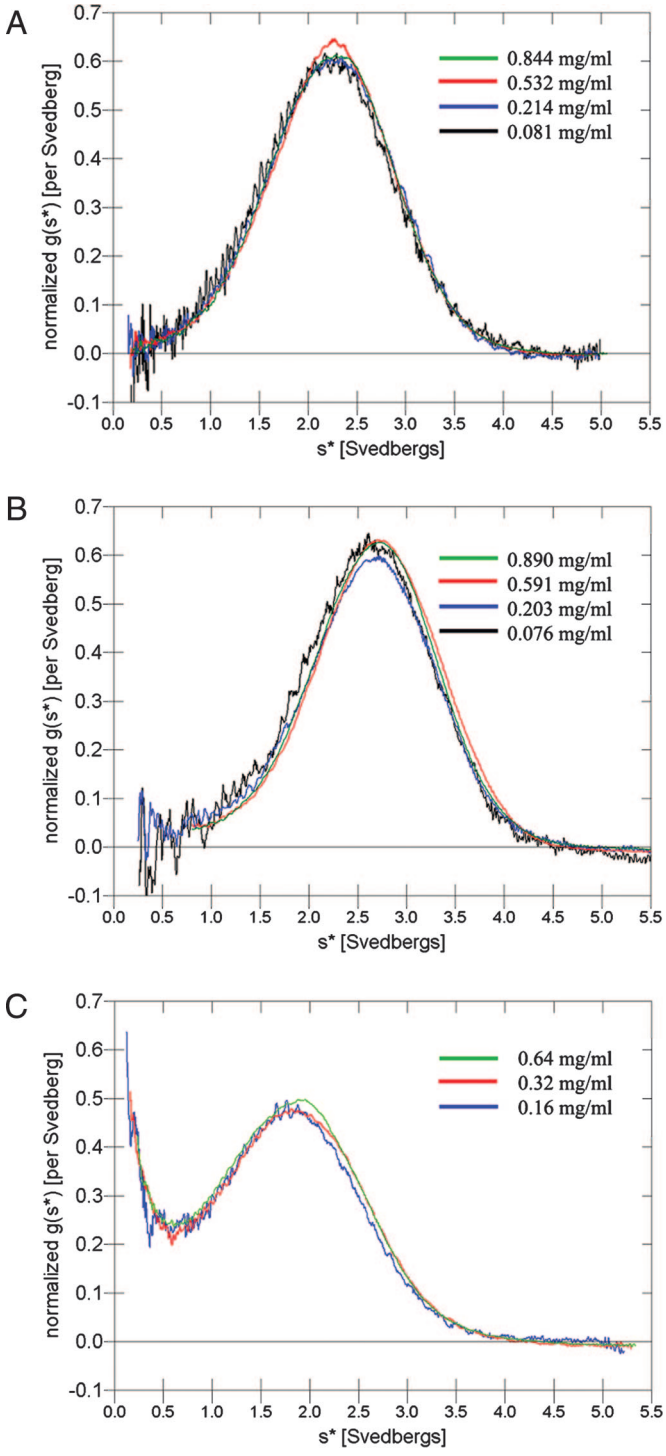

Fig. 1. Oligomeric state of CD84 and CD84-T99A mutation. Overlay of the normalized g(s*) plots from DcDt+ analysis of the sedimentation velocity data at different concentrations: CD84 IgV domain (*A*), CD84 IgVC domain (*B*), and CD84-T99A (*C*).

on the C″D loop from molecule A with D90, N92 on the F strand, and T99 on the G strand from molecule B. The strand-to-strand interactions include contacts between the side chains of A33 and T35 on the C strand of molecule A and side-chain and main-chain atoms on the C and C′ strands from molecule B, as well as side-chain-to-main-chain contacts involving Y42 and A41 from opposing molecules. In addition, a loop-to-loop interaction

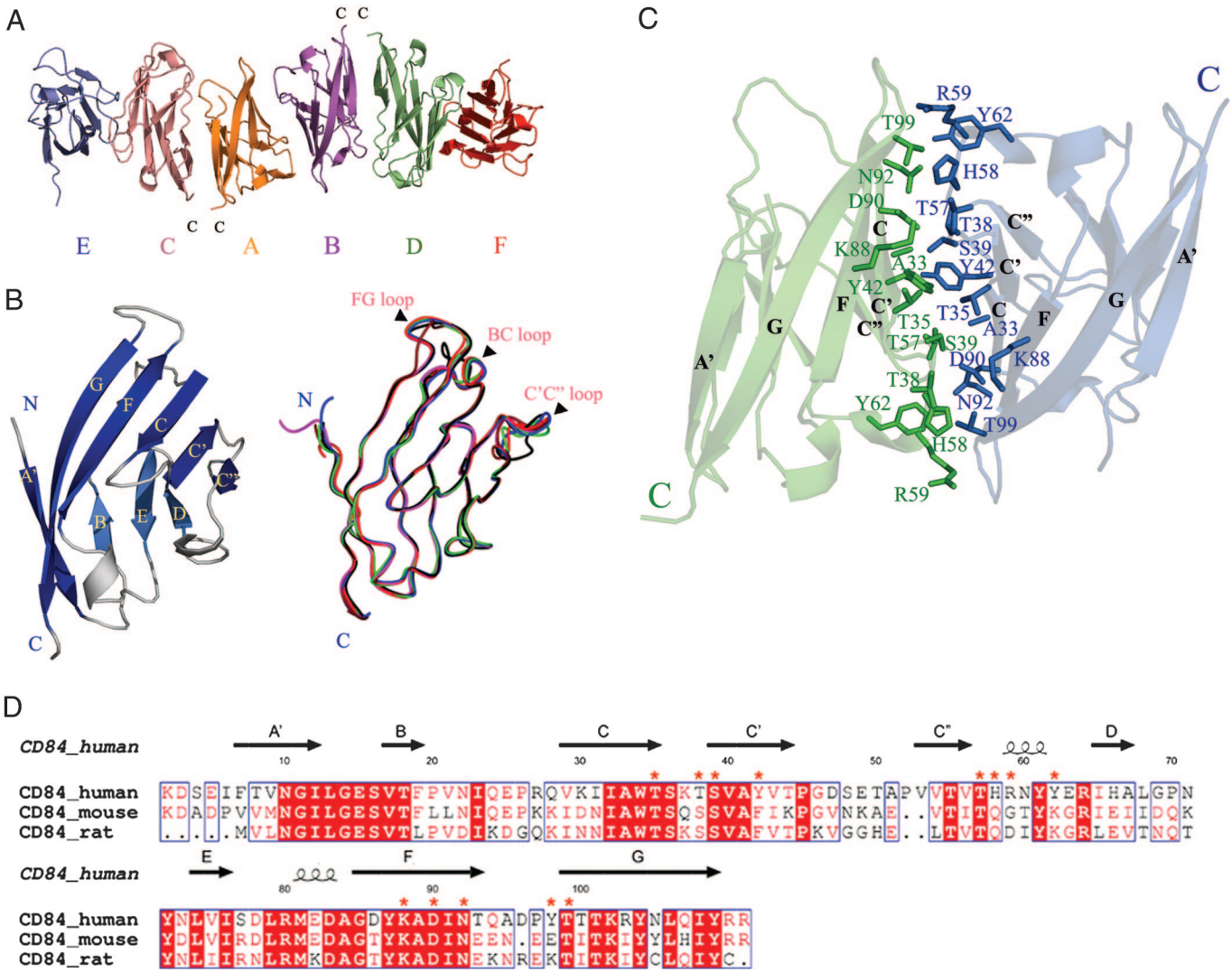

Fig. 2. Overall structure of CD84 IgV domain. (*A*) The ribbon diagram of the overall structure of the six independent CD84 molecules in the asymmetric unit. Molecules A, B, C, D, E, and F are colored orange, magenta, salmon, green, blue, and red, respectively. The C termini of molecules A, B, C, and D are labeled with C. (*B*) (*Left*) Structure of monomeric CD84 IgV domain. The monomer is a two-layer β-sandwich, with front (blue) and back (light blue) sheets composed of A′GFCC′C″ and BED strands, respectively. (*Right*) The ribbon diagram of the superimposition of six CD84 monomers in one asymmetric unit. The six molecules overlap very well, with the greatest deviations in the FG, BC, and C′C″ loops. (*C*) The CD84 head-to-tail dimer interface. Residues at the head-to-tail dimer interface from molecules A and B are labeled with green and blue, respectively. (*D*) The multiple sequence alignment of the human, mouse, and rat CD84 IgV domains. The residues with >50% conservation are colored in red; identical residues are highlighted in bold white with red shade. The asterisks mark residues in the CD84 homophilic dimer interface. The secondary structure of CD84 IgV domain is shown above the alignment.

is provided by the side and main chains of R59 and P97, respectively. Because of the twofold symmetry of the homophilic dimer, there are two independent, symmetry-related sets of the above interactions. Notably, the symmetry-related equivalents of Y42 from the C′ strand of each molecule form a single stacking interaction that demarks the approximate middle of the interface. The interfaces in all three head-to-tail dimers are generally similar, and a number of the contributing residues are highly conserved (Fig. 2*D*).

Molecules A and C contribute eight residues to the side-to-side dimer interface, which buries ≈1,200 Å^2 of the surface area (SI Fig. 6 and SI Table 2). The side-to-side dimer interface has fewer direct hydrogen bonds (eight in the AC complex, three in the BD complex, and seven in the FE′ complex) than the head-to-tail dimer interface (14 in the AB complex), although more water-mediated polar interactions are present in the side-to-side dimer interface. The head-to-tail dimer has a significantly higher shape complementarity (Sc) than the side-to-side dimer, with average Sc values of 0.68 and 0.5, respectively (Sc values of 1.0 and 0 correspond to perfect complementarity and complete mismatch, respectively). The Sc value of 0.68 is slightly lower than protein–oligomer and protease–inhibitor interfaces (0.7–0.76) and is similar to that observed for antibody–antigen interfaces (0.65–0.68) (19).

CD84 Head-to-Tail Dimer Is the Predominant Dimer in Solution. Based on their conservation and predicted contribution to the head-to-tail binding interface, 11 residues were mutated to alanine (T35, S39, Y42, T57, H58, R59, Y62, K88, D90, N92, and T99) and one to aspartic acid (Y42D) in the full-length ectodomain construct (CD84 IgVC domain). All mutants were expressed in *Escherichia coli* and successfully refolded *in vitro*, except for S39A. As judged by gel-filtration chromatography, seven mutant proteins (T35A, T57A, H58A, D90A, N92A, T99A, and Y42D) exhibited behavior consistent with a hydrodynamic radius significantly smaller than that of the wild-type protein (SI Fig. 7).

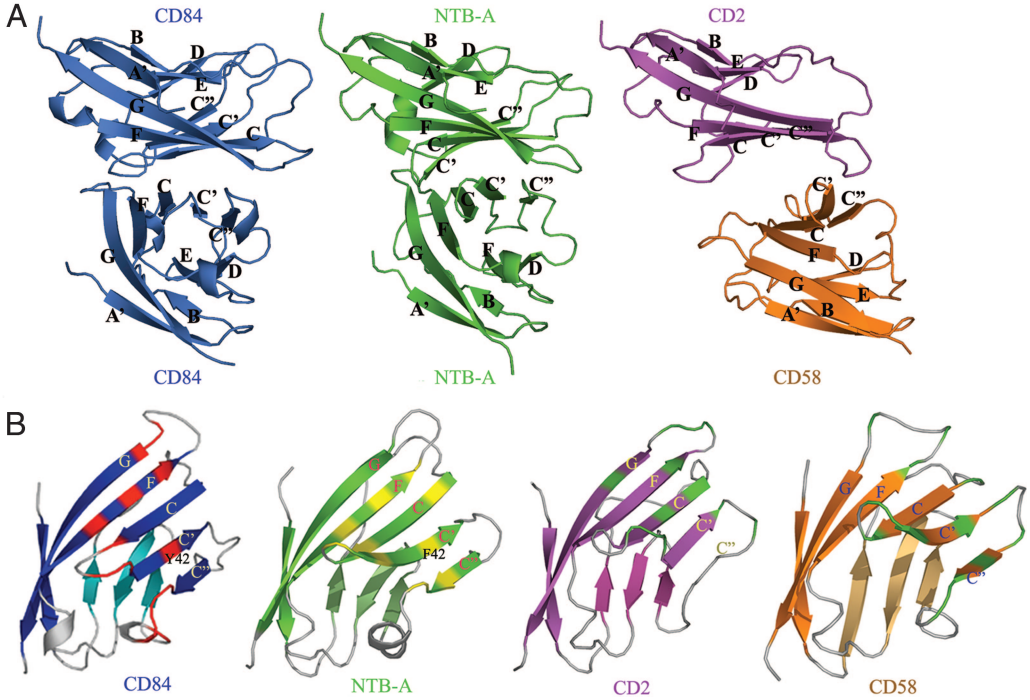

Fig. 3. Comparison of CD84, NTB-A, and CD2-CD58. (*A*) The ribbon diagram presentation of the CD84 homophilic dimer, NTB-A homophilic dimer, and CD2–CD58 heterophilic dimer. The upper NTB-A and CD2 molecules are superimposed with the upper CD84 molecule. (*B*) The ribbon diagram presentation of the the CD84, NTB-A, CD2, and CD58 monomers. The residues involved in the CD84 or NTB-A homophilic dimer are colored with red and orange, respectively. The residues involved in the CD2–CD58 heterophilic dimers are colored green.

One of these mutants, T99A, was examined by sedimentation velocity analysis. The superimposition of the normalized g(s*) plots is strong evidence that, over the concentration range examined, there is no reversible association occurring (Fig. 1*C*). Data for CD84-T99A were analyzed with Sedphat version 4.04 by using the hybrid model of a sedimentation coefficient distribution, c(s), plus a single ideal species (16) and yielded a molecular mass of 21.8 kDa. These results indicated that over the concentration range examined CD84-T99A is monomeric (expected monomer molecular mass of 22.4 kDa). It is likely that the T35A, T57A, H58A, D90A, and N92A mutations also disrupted the head-to-tail dimer interface because the corresponding proteins exhibited chromatographic behavior similar to that of T99A. The Y42A, R59A, Y62A, and K88A mutant proteins exhibited chromatography properties similar to the wild-type protein (SI Fig. 7), suggesting a lesser effect on the homophilic dimerization. Notably, the Y42D mutation, which likely introduces an unfavorable electrostatic interaction between symmetry-related side chains across the interface, resulted in the disruption of the dimer (SI Fig. 7). The N10A and Q24A mutants located in the crystallographically observed side-to-side dimer interface had no effect on the chromatographic behavior (data not shown), arguing against the existence of the side-to-side dimer in solution. Taken together, these results support a model in which the head-to-tail dimer is the predominant oligomeric state of CD84 in solution.

Discussion

Gel-filtration and AUC data showed that both the CD84 IgV and CD84 IgC domains exist as tight dimers in solution, with K_d in the submicromolar range. The crystal structure of the CD84 IgV domain suggested two potential dimerization modes; however, biophysical, biochemical, and mechanistic considerations support the head-to-tail dimer as the physiologically relevant species. The head-to-tail dimer buries a larger interface than the side-to-side dimer (≈1,400 vs. 1,200 Å^2) and exhibits significantly higher shape complementarity (Sc values of 0.68 vs. 0.5). Mutagenesis experiments also support the existence of the head-to-tail dimer because the mutation of residues in the putative head-to-tail dimer interface (T35A, T57A, H58A, D90A, N92A, T99A, and Y42D) resulted in solution behavior consistent with the disruption of the dimer (SI Fig. 7). The CD84 head-to-tail dimer exhibited the same twofold symmetrical organization recently reported for the full NTB-A ectodomain and, most important, is consistent with the formation of an intercellular (T cell-APC) homophilic dimer that can support signaling (see below) (12).

The structures of the CD84 IgV domain, the complete NTB-A ectodomain, and the CD2–CD58 complex provide the basis for examining the features that define and distinguish the homophilic and heterophilic interactions within the CD2/SLAM family. The CD84 and NTB-A homophilic dimers exhibit several common features that contribute to the binding interface. Multiple side-chain functionalities contributed from the F strand form hydrogen bonds across the interface (Fig. 3*B*). The equivalent residues in F strands from Ly-9 and CRACC, except for G58 in CRACC, have the capability of participating in hydrogen bond interactions through their side chains, suggesting that similar contacts contribute to all SLAM family homophilic interactions. In addition, an aromatic residue (F42 and Y42 in the C′ strand from NTB-A and CD84, respectively) and its symmetry mate participate in a hydrophobic stacking interaction that marks the approximate center of these homophilic interfaces. The equivalent residue in Ly-9, F42, is likely to participate in similar interactions (SI Fig. 8).

Although the CD84 and NTB-A dimers exhibit considerable similarities in their overall organization, there are also detailed differences. The CD84 dimer interface is predominately hydrophilic, in contrast to the NTB-A dimer interface, which contains a considerable number of hydrophobic residues (SI Fig. 9). In addi-

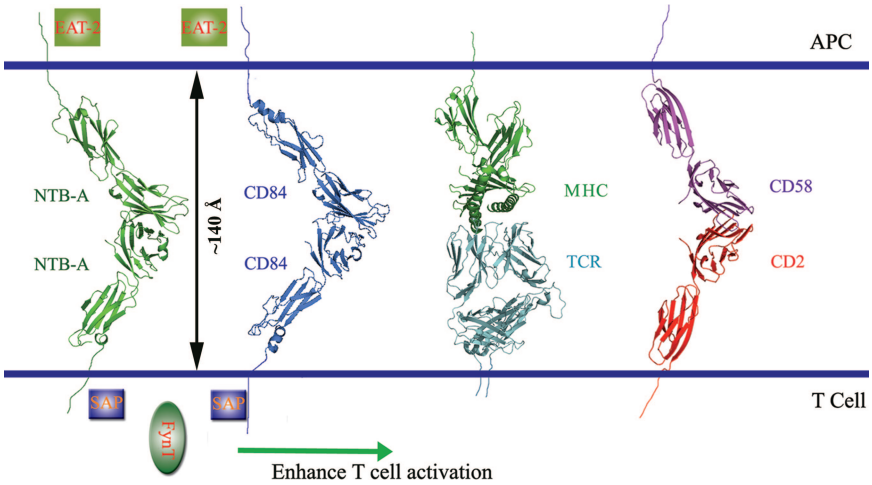

Fig. 4. Model of human CD84 involved in T cell activation. The ribbon diagram representation of the model of the CD84 homophilic interaction, NTB-A homophilic interaction, and CD2–CD58 heterophilic interaction between T cell and APC. The MHC–TCR complex is also shown for a comparison of molecular dimensions.

tion, the dimer interface of NTB-A is less planar than that of CD84 because the C′ strand and the CC′ loop of NTB-A bend away from the back sheet (i.e., toward the dimer interface). In NTB-A, H54 from the C′′ strand contacts F30 and Y42 from the symmetry-related C and C′ strands, respectively. However, in CD84, the C′′ strand is shifted away from the dimer interface, which prevents contacts with the C and C′ strands on the associating molecule. In addition, the side chain of the first residue (T99) of the G strand in CD84 forms a hydrogen bond with the side chain of R59 in the C′′D loop from the associating molecule. In NTB-A, this interaction is absent because the corresponding residue is an alanine. The significant differences in the chemical and physical determinants that contribute to the CD84 and NTB-A interfaces suggest a mechanism to prevent the formation of undesired heterodimers among the SLAM family receptors.

Differences in the organization of the homophilic and heterophilic assemblies are best appreciated by the superposition of one molecule from each complex and the observation of the deviation in the placement of the second interacting molecule. Although there is only an ≈2-Å shift between the second CD84 and NTB-A molecules, CD58 deviates significantly (≈10 Å) from the second CD84 and NTB-A molecules (Fig. 3*A*). Of particular note is the lack of a significant electrostatic contribution to the homophilic interactions because there are fewer charged residues involved in the CD84 and NTB-A homophilic interfaces compared to the heterophilic CD2-CD58 interface. Instead, hydrogen bonds and van der Waals contacts provide most of the energy for the stablization of the CD84 and NTB-A homophilic dimers. The symmetric CD84 and NTB-A homophilic dimer interfaces exhibit high surface complementarity (0.68 for both molecules), in contrast to the relative poor shape complementarity of the CD2–CD58 interface (0.58). However, the magnitude of the interfaces are similar among the CD84, NTB-A, and CD2–CD58 dimers, with total buried surface areas of 1,460 Å^2, 1,583 Å^2, and 1,422 Å^2, respectively.

A model of the entire CD84 ectodomain homophilic dimer can be constructed on the basis of the full-length human NTB-A ectodomain crystal structure. Based on sequence and structural considerations, all SLAM family members possess a five-residue segment that connects the IgV and IgC domains. Furthermore, all family members possess hydrophobic residues at the equivalent positions of Tyr-105 and Val-179 in CD84, which likely participate in hydrophobic interactions that influence the relative orientation of the IgV and IgC domains. Finally, Asn-177 in the FG loop, which participates in side-chain-to-main-chain hydrogen bonds at the IgV–IgC interface, is invariant in the SLAM family. These interactions likely cause all two-domain SLAM family members to adopt a similar interdomain geometry, which results in a rodlike monomer similar to that observed in NTB-A (12). As suggested for NTB-A, based on this overall ectodomain organization, CD84 molecules contributed from the T cell and APC associate in an orthogonal fashion to form a kinked dimer, spanning an end-to-end distance of ≈140 Å. This distance is comparable to the linear dimensions of other pairs of signaling molecules within the immunological synapse (e.g., TCR/pMHC, CD2/CD58, and CTLA-4/B7) and is consistent with a size-based mechanism for localizing similarly sized molecular pairs to the central zone of the immunological synapse. These common molecular dimensions provide an opportunity for all two-domain SLAM family receptors to colocalize within the immunological synapse and bridge the T cell and APC (Fig. 4).

Our AUC data demonstrate that CD84 self-associates with a K_d in the submicromolar range. The homophilic affinity is in contrast to the NTB-A and CD150 homophilic interactions, which are characterized by K_d of 2 μM and 200 μM, respectively (12, 13). The three orders of magnitude range in homophilic affinities suggest a mechanistic basis for the overlapping, but distinct, biological functions exhibited by the SLAM family members. This notion is reminiscent of the optimal dwell times of the TCR–MHC interaction required for efficient T cell activation (20). The SLAM family receptors are also distinguished by unique sequences in the cytoplasmic tails responsible for binding adaptor and signaling molecules. The importance of these differences is highlighted by the recent report that NTB-A splice variants possessing distinct numbers of immunoreceptor tyrosine-based switch motif exhibit different signaling capabilities in B cells (21).

Our crystallographic and biochemical analyses support a model in which CD84 forms a kinked homophilic dimer that bridges the T cell and APC. Analytical ultracentrifugation studies also indicated that there were no higher oligomeric states beyond the dimer, suggesting that ligand binding-induced oligomerization, such as that proposed for the growth factor receptors, is unlikely to be part of the signaling mechanism used by CD84. Furthermore, the compact features of the IgV domain do not appear to be compatible with a conformational change that could facilitate downstream signaling. Therefore, we propose a model in which the homophilic association of CD84 molecules, on interacting T cells and APCs, induces the redistribution of freely diffusing CD84 molecules to the immunological synapse, resulting in a local enrichment of CD84 and its

associated binding partners (i.e., SAP, EAT-2). This enrichment triggers a series of molecular events, which ultimately result in the enhancement of T cell activation and IFN-γ secretion. Given the overall sequence and structural similarity, we propose that similar mechanisms are used by all SLAM family receptor members.

Experimental Procedures

Cloning, Expression, and Purification of CD84 IgV and IgC Domain Proteins. The extracellular IgV domain (110 amino acid residues excluding the initiator Met) and the entire ectodomain, composed of a membrane-distal IgV and a membrane-proximal IgC (IgVC; 199 amino acid residues excluding the initiator Met) of CD84, were expressed and refolded as described for B7–2 (22). Briefly, CD84 IgV and IgC domains were expressed in *E. coli* and refolded from inclusion bodies *in vitro*. Refolded IgV and IgC proteins were chromatographed on Superdex G-75 and Superdex 200 gel-filtration columns, respectively, followed by MonoQ chromatography. Expression and purification of selenomethionine-substituted IgV was similar to that described by Zhang *et al.* (22). The QuikChange site-directed mutagenesis kit (Stratagene, La Jolla, CA) was used to generate a series of point mutations of CD84. Mutant sequences were confirmed by DNA sequencing, and the proteins were purified as described for the native material.

Crystallization and Data Collection. Diffraction quality crystals of native and selenomethionine-substituted CD84 IgV domain were obtained by hanging drop vapor diffusion at 21°C by mixing 2 μl of 12 mg/ml protein in 10 mM (pH 8.5) Tris·HCl buffer with 1 μl of reservoir solution composed of 20% PEG3350, 0.3 M $MgCl_2$, and 0.1 M Hepes (pH 7.5) and equilibrating samples against reservoir solution for 2 days. Diffraction was consistent with the space group $C222_1$ (*a*, 61.02 Å; *b*, 170.77 Å; *c*, 148.68 Å; and six molecules of the CD84 IgV domain in the asymmetric unit). Crystals were briefly transferred to reservoir solution containing 20% PEG400 and flash-cooled in a nitrogen stream (Oxford Cryosystems, Oxford, U.K.) at 100°K. Native data were collected to a resolution of 2.0 Å from a single crystal at the National Synchrotron Light Source X-29 beamline. MAD data (wavelengths 0.97940, 0.97970, and 0.96100 Å) were collected to a resolution of 2.4 Å from a single selenomethionine-substituted crystal at the X-9A beamline. Intensities were integrated with HKL2000 (23) and reduced to amplitudes by using TRUNCATE (24) (SI Table 3). Heavy atom positions were determined with SOLVE (25) and SHELX (26). Initial phases were calculated with SOLVE and improved by using density modification methods in RESOLVE (27). The initial atomic model of the CD84 IgV domain was built with ARP/wARP (28), except for flexible loops, which required manual intervention. Crystallographic refinement used CNS1.1 (29) and Refmac (30). Model building was initially performed with O (31) and later with Coot (32). All other calculations used the CCP4 program suite (24). The quality of the final structure was verified with composite omit maps, and the stereochemistry was checked with PROCHEK (33). Figures were produced with PyMOL (DeLano Scientific LLC, Palo Alto, CA).

Multiple-sequence alignments were performed with MultAlin (34) and rendered with ESPript (35). Hydrogen bond distances, buried surface area, and shape complementarity were calculated by the programs CONTACT (with a cutoff of 3.5 Å), AREAIMOL, and SC, respectively, from the CCP4 package (24).

Analytical Ultracentrifugation. The wild-type ectodomain, IgV domain, and T99A ectodomain mutant of CD84 proteins were exchanged into a buffer containing 20 mM Tris·HCl (pH 8.5) and 50 mM NaCl. For each sample, three or four concentrations (0.84–0.081 mg/ml for IgV, 0.89–0.076 mg/ml for ectodomain, and 0.64–0.15 mg/ml for the T99A mutant) were used in sedimentation velocity experiments. The data were collected at 20°C and centrifuged at 224,000 $\times$ *g* in a Beckman Coulter (Fullerton, CA) XL-I, and interference scans were acquired at 1-min intervals for 5 or 7 h depending on the sample. The AUC data were analyzed with the DcDt+ program of John Philo (version 1.99.1990) (14, 15). The data were also analyzed globally by using the direct boundary modeling program Sedphat (16), which allows the user to fit the data to various association schemes by using multiple as well as individual data sets.

We thank the staff of the X9A and X29 beam lines at the National Synchrotron Light Source for the help, and Drs. C. Terhorst, T. DiLorenzo, and K. Chattopadhyay for critical reading of the manuscript. This work was supported by National Institutes of Health Grant AI07289 (to S.G.N. and S.C.A.).

1. Veillette A (2006) *Nat Rev Immunol* 6:56–66.
2. Kingsbury GA, Feeney LA, Nong Y, Calandra SA, Murphy CJ, Corcoran JM, Wang Y, Prabhu Das MR, Busfield SJ, Fraser CC, Villeval JL, *et al.* (2001) *J Immunol* 166:5675–5680.
3. Fraser CC, Howie D, Morra M, Qiu Y, Murphy C, Shen Q, Gutierrez-Ramos JC, Coyle A, Kingsbury GA, Terhorst C (2002) *Immunogenetics* 53:843–850.
4. Engel P, Eck MJ, Terhorst C (2003) *Nat Rev Immunol* 3:813–821.
5. Clayton LK, Ramachandran H, Pravtcheva D, Chen YF, Diamond DJ, Ruddle FH, Reinherz EL (1988) *J Immunol* 140:3617–3621.
6. Dupre L, Andolfi G, Tangye SG, Clementi R, Locatelli F, Arico M, Aiuti A, Roncarolo M-G (2005) *Blood* 105:4383–4389.
7. Wang N, Satoskar A, Faubion W, Howie D, Okamoto S, Feske S, Gullo C, Clarke K, Sosa MR, Sharpe AH, Terhorst C (2004) *J Exp Med* 199:1255–1264.
8. Graham DB, Bell MP, McCausland MM, Huntoon CJ, van Deursen J, Faubion WA, Crotty S, McKean DJ (2006) *J Immunol* 176:291–300.
9. Howie D, Laroux FS, Morra M, Satoskar AR, Rosas LE, Faubion WA, Julien A, Rietdijk S, Coyle AJ, Fraser C, Terhorst C (2005) *J Immunol* 174:5931–5935.
10. Martin M, Romero X, de la Fuente MA, Tovar V, Zapater N, Esplugues E, Pizcueta P, Bosch J, Engel P (2001) *J Immunol* 167:3668–3676.
11. Nanda N, Andre P, Bao M, Clauser K, Deguzman F, Howie D, Conley PB, Terhorst C, Phillips DR (2005) *Blood* 106:3028–3034.
12. Cao E, Ramagopal UA, Fedorov A, Fedorov E, Yan Q, Lary JW, Cole JL, Nathenson SG, Almo SC (2006) *Immunity* 25:559–570.
13. Mavaddat N, Mason DW, Atkinson PD, Evans EJ, Gilbert RJC, Stuart DI, Fennelly JA, Barclay AN, Davis SJ, Brown MH (2000) *J Biol Chem* 275:28100–28109.
14. Philo JS (2006) *Anal Biochem* 354:238–246.
15. Philo JS (2000) *Anal Biochem* 279:151–163.
16. Schuck P (2003) *Anal Biochem* 320:104–124.
17. Wang J-H, Smolyar A, Tan K, Liu J-H, Kim M, Sun Z-YJ, Wagner G, Reinherz EL (1999) *Cell* 97:791–803.
18. Ames JB, Vyas V, Lusin JD, Mariuzza R (2005) *Biochemistry* 44:6416–6423.
19. Lawrence MC, Colman PM (1993) *J Mol Biol* 234:946–950.
20. Kalergis AM, Boucheron N, Doucey M-A, Palmieri E, Goyarts EC, Vegh Z, Luescher IF, Nathenson SG (2001) *Nat Immunol* 2:229–234.
21. Kumar KR, Li L, Yan M, Bhaskarabhatla M, Mobley AB, Nguyen C, Mooney JM, Schatzle JD, Wakeland EK, Mohan C (2006) *Science* 312:1665–1669.
22. Zhang X, Schwartz J-CD, Almo SC, Nathenson SG (2002) *Protein Expression Purif* 25:105–113.
23. Otwinowski Z, Minor W (1997) in *Methods in Enzymology* (Academic, New York), Vol 276, pp 307–326.
24. Collaborative Computational Project N (1994) *Acta Crystallogr* 50:760–763.
25. Terwilliger TC, Berendzen J (1999) *Acta Crystallogr* 55:849–861.
26. Sheldrick GM, Schneider TR (1997) in *Methods in Enzymology* (Academic, New York), Vol 277, pp 319–343.
27. Terwilliger T (2000) *Acta Crystallogr* 56:965–972.
28. Lamzin VS, Wilson KS, Perrakis A (2001) in *Int. Tables for Crystallography*: *Vol. F. Crystallography of Biological Macromolecules*, eds Rossmann MG, Arnold E (Kluwer, Dordrecht, The Netherlands), pp 720–722.
29. Brunger AT, Adams PD, Clore GM, DeLano WL, Gros P, Grosse-Kunstleve RW, Jiang J-S, Kuszewski J, Nilges M, Pannu NS, *et al.* (1998) *Acta Crystallogr* 54:905–921.
30. Murshudov GN, Vagin AA, Dodson EJ (1997) *Acta Crystallogr* 53:240–255.
31. Jones TA, Zou JY, Cowan SW, Kjeldgaard M (1991) *Acta Crystallogr* 47:110–119.
32. Emsley P, Cowtan K (2004) *Acta Crystallogr* 60:2126–2132.
33. Laskowski RA, MacArthur MW, Moss DS, Thornton JM (1993) *J Appl Cryst* 26:283–291.
34. Corpet F (1988) *Nucleic Acids Res* 16:10881–10890.
35. Gouet P, Courcelle E, Stuart DI, Metoz F (1999) *Bioinformatics* 15:305–308.